ELSEVIER

Contents lists available at ScienceDirect

Ceramics International

journal homepage: www.elsevier.com/locate/ceramint





Mechanical properties of the fuel electrode support for protonic ceramic fuel and electrolysis cells

Yuan Zeng ^{a,b,*}, Jürgen Malzbender ^c, Olivier Guillon ^{a,b,d}, Mariya E. Ivanova ^a, Norbert H. Menzler ^{a,b}

- a Forschungszentrum Jülich GmbH, Institute of Energy Materials and Devices IMD-2: Materials Synthesis and Processing, 52425, Jülich, Germany
- b RWTH Aachen University, Institute of Mineral Engineering (GHI), Department of Ceramics and Refractory Materials, 52064, Aachen, Germany
- Forschungszentrum Jülich GmbH, Institute of Energy Materials and Devices IMD-1: Structure and Function of Materials, 52425, Jülich, Germany
- ^d Jülich-Aachen Research Alliance: JARA-Energy, 52425, Jülich, Germany

ARTICLE INFO

Handling Editor: Dr P. Vincenzini

Keywords:
Proton-conducting ceramic cells
BZCY/NiO
Fuel electrode support
Mechanical properties
Bending strength
Weibull analysis

ABSTRACT

This work investigates the mechanical properties of $BaZr_{0.65}Ce_{0.2}Y_{0.15}O_{3-\delta}/NiO$ (BZCY/NiO) fuel electrode supports processed via tape casting and sintered at varying temperatures (1400–1500 °C). Bending strength and elastic modulus were evaluated using the ring-on-ring testing method. A strong inverse correlation was observed between porosity and both bending strength and elastic modulus, well described by exponential decay functions. Weibull statistical analysis further highlighted increased strength variability at higher sintering temperatures due to heterogeneous microstructural defects. Post-reduction samples exhibited significant mechanical degradation, raising concerns for their structural integrity in practical applications. High-temperature testing showed no strength deterioration at 500–600 °C, indicating stable performance under operating conditions. Comparative analysis with yttria-stabilized zirconia (YSZ)/NiO fuel electrode supports emphasized the mechanical short-comings of the current BZCY-based systems. This work provides foundational insights for improving mechanical robustness of proton-conducting ceramic electrochemical cell electrode supports.

1. Introduction

In the context of the urgent global need for energy transition and carbon neutrality, solid-state fuel and electrolysis cells, which can reversibly convert electrical energy and chemical energy, have gained increasing attention for their vital role in sustainable energy systems. Proton-conducting ceramic electrochemical cells (PCCs) are an emerging and highly attractive technology that can operate at lower temperatures ($<600\,^{\circ}$ C) compared to oxide-ion conductors ($\sim700-850\,^{\circ}$ C) [1–3]. This lower-temperature operation enables the use of more cost-effective materials, improves system durability, and enhances integration with intermittent renewable energy sources. As a result, PCCs are seen as a key pathway toward high-efficiency, flexible, and decentralized energy conversion technologies.

Most cell configurations still employ the strategy of using fuel electrode supports [4–6]. This approach has a significant advantage in that it allows for the fabrication of thinner electrolyte layers, consequently enabling the electrolyte to retain high ionic conductivity at lower

temperatures. In this design, the fuel electrode support provides the mechanical strength for the entire cell. A robust support layer is necessary since the cell faces many mechanical strength challenges throughout its fabrication and operational life, including thermal cycling, and long-term service [7-10]. To ensure reliability and durability, the cells must possess sufficient mechanical strength from the outset - capable of withstanding the rigors of stack integration and long-term deployment. During operation, the cells (single or in stack) need to withstand stresses caused by high temperatures, thermal gradients, thermal cycling, and other related factors. Even minor cracks can propagate over time, ultimately leading to the failure of the entire stack and compromising overall system performance. To address these challenges, it is crucial to enhance the mechanical strength of the substrate to increase the maximum tolerable stress threshold. However, this presents a demanding design trade-off for the fuel electrode support layer, which must maintain sufficiently high porosity to ensure effective gas

The fuel electrode support typically has the same composition as the

E-mail address: y.zeng@fz-juelich.de (Y. Zeng).

^{*} Corresponding author. Forschungszentrum Jülich GmbH, Institute of Energy Materials and Devices IMD-2: Materials Synthesis and Processing, 52425, Jülich, Germany.

fuel electrode, consisting of a certain proportion of electrolyte material and NiO (reduced to Ni during operation). For example, in the case of oxygen ion conductors, the fuel electrode support is composed by yttriastabilized zirconia (YSZ) and NiO. In the research conducted over the past decades, YSZ/NiO(Ni) compound has proven its reliable mechanical performance as a support layer for solid oxide cells (SOC), even during extended operational periods [11]. However, in the case of PCCs utilizing $BaZr_xCe_yY_{1-x-y}O_3$ (BZCY)/NiO(Ni)-based fuel electrode supports, which remain at a relatively early stage of research and development, mechanical failures are frequently observed during laboratory handling, including sample transfer and test assembly. Despite the substantial increase in research on PCC in recent years, the focus has primarily been on their material development and electrochemical performance [12-15]. In contrast, studies addressing the structural integrity and mechanical properties of BZCY/NiO(Ni)-based fuel electrode supports remain limited and relatively underexplored [16,17].

Bending strength is an important indicator of a material's capacity to withstand mechanical loads [18,19]. It represents the maximum stress that a component can endure during a bending test before fracture or failure occurs. It is a highly relevant metric for assessing the mechanical reliability of PCCs. There are several methods for testing bending strength, such as traditional three-point or four-point bending tests [20, 21]. However, these techniques all face issues with stress concentration effects, making them less suitable for thin-sheet samples. In contrast, the ring-on-ring test offers significant advantages when testing thin-sheet PCC samples [22,23]. By applying load through ring-shaped supports, this method provides a more uniform stress distribution, making it particularly well-suited for thin, circular samples.

In this work, we systematically investigate the mechanical properties, particularly the bending strength and elastic modulus of BZCY/NiO fuel electrode supports, examining the effects of varying sintering temperature as well post-reduction conditions. Considering the superior thermochemical stability of high Zr content BZCY compositions and the reduced risk of secondary phase formation at moderate Y substitution levels [24–26], BaZr_{0.65}Ce_{0.2}Y_{0.15}O_{3- δ} was selected as the focus of this study. The influence of porosity on mechanical performance was analyzed through scanning electron microscope (SEM) image analysis and quantitatively modeled using exponential decay relationships. Fracture origins and microstructural failure mechanisms were further revealed through SEM-based fractography. Finally, we evaluated the mechanical reliability of the supports by Weibull statistics analysis and benchmarked their performance against conventional YSZ/NiO-based systems. This study aims to address the knowledge gap in the mechanical reliability of BZCY-based fuel electrode supports and provide practical insights and guidance for future structural optimization and material design.

2. Experimental procedure

2.1. Samples preparation

The $BaZr_{0.65}Ce_{0.2}Y_{0.15}O_{3-\delta}/NiO$ (BZCY/NiO) fuel electrode supports were fabricated via tape casting, followed by de-binding and sintering. Commercial NiO (Vogler, Netherlands) was used as received, while BZCY powder was synthesized in-house through a conventional solid-state reaction method. Raw powders of $BaCO_3$, ZrO_2 , CeO_2 , and Y_2O_3 (Sigma Aldrich, purity grade of 99 %) were accurately weighed and homogenized in ethanol using a tumbler mixer for 24 h. The resulting slurry was subsequently dried at 80 °C for 24 h to obtain a uniform precursor powder. The dried powder was collected and calcined at 1100 °C for 10 h to ensure phase formation. Prior to paste preparation for tape casting, the powder was sieved using a $100~\mu m$ mesh. For the casting slurry preparation, 40 wt% of BZCY and 60 wt% of NiO were mixed. An appropriate amount of dispersant, binder, and plasticizer was added, and the mixture was thoroughly homogenized using a centrifugal planetary mixer. The prepared slurry was then tape cast, and the

resulting dried tape with thickness of 450 μm was punched into round specimens with a diameter of 18 mm. De-binding was carried out at 900 °C for 1 h. The samples after de-binding were subsequently sintered at 1400 °C, 1450 °C, and 1500 °C for 3 h on sacrificial powder in the Al $_2$ O $_3$ crucible, respectively, and are hereafter denoted as 1400, 1450, and 1500, respectively. The samples sintered at 1450 °C were further subjected to a reduction treatment in an Ar + 3 vol% $\rm H_2$ atmosphere and denoted as 1450 re.

2.2. Characterization techniques

Phase composition of the sintered samples was analyzed using a Bruker D4 Endeavour X-ray diffractometer with Cu-K α radiation. The microstructure of both polished specimens and fracture surfaces was observed using a scanning electron microscope (SEM, TM3000, Hitachi, Japan). Porosity analysis was conducted using ImageJ/Fiji software, which identifies pores based on distinct grayscale contrast between pores and solid phases (particles), and calculates the area fraction of pore regions.

Elastic modulus and bending strength were evaluated using a ring-on-ring test configuration (Instron 1362-DOLI, Warren, USA). Disc-shaped samples with a diameter of around 14.5 mm were tested using a loading ring and support ring with diameters 3.43 mm and 9.99 mm, respectively. The loading rate was set to $100 \, \text{N/min}$ and a Poisson's ratio of 0.24 was assumed for the calculation. For each sample series, 25 samples were tested at room temperature to determine the average elastic modulus, average bending strength, characteristic strength, and Weibull modulus via linear regression analysis. Additionally, three samples per condition were tested at elevated temperatures (500 °C and 600 °C) in both air and a reducing atmosphere (3 vol% $\,\text{H}_2/\text{Ar})$ to determine average fracture stresses. For further details on the setup used, data analysis procedure, and calculation methods, the reader is referred to previous studies [27,28].

3. Results and discussion

The XRD patterns of the fuel electrode supports sintered at different temperature and post-reduction are shown in Fig. 1. Analysis of the diffraction patterns confirms that all samples, regardless of the sintering temperature, predominantly consist of the cubic perovskite phase BZCY alongside the NiO phase. No secondary or impurity phases were

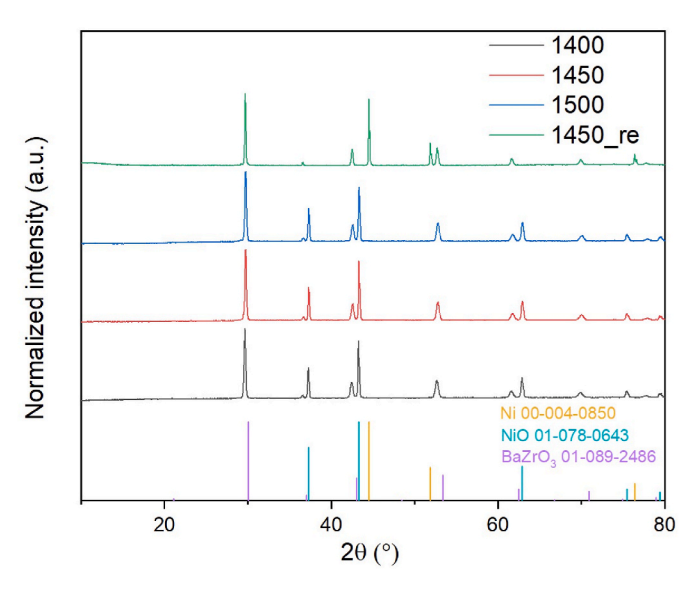


Fig. 1. XRD patterns of BZCY/NiO fuel electrode supports sintered at 1400 $^{\circ}$ C, 1450 $^{\circ}$ C and 1500 $^{\circ}$ C. The sample labeled 1450-re refers to the 1450 $^{\circ}$ C-sintered sample after reduction in 3 vol% H₂/Ar at 900 $^{\circ}$ C.

detected, indicating high phase purity. The sample sintered at $1450\,^{\circ}\mathrm{C}$ was selected for further reduction. Post-reduction XRD analysis reveals that NiO is successfully transformed into metallic Ni, with no significant formation of any additional phases. This confirms that all samples maintain their structural integrity and can be classified as "XRD-pure".

Fig. 2 shows the SEM-BSE (backscattered electron) images of the BZCY/NiO(Ni) fuel electrode supports after various thermal and chemical treatment processes. In backscattered mode, regions with elements of higher atomic numbers appear brighter. Accordingly, in these micrographs, black areas represent pores, bright areas correspond to BZCY phases, and the intermediate gray areas indicate NiO or metallic Ni phases, depending on the treatment.

It can be observed that with the increase in sintering temperature, the porosity gradually decreases. At these three sintering temperatures, there is no significant difference in the size and morphology of the NiO particles. The BZCY particles seem to exhibit a better connection (enhanced necking) and densification at higher sintering temperatures, suggesting improved interparticle bonding. Furthermore, the porosity of 1450_re increases compared to the unreduced 1450 °C sample due to the reduction-induced phase transformation of NiO to metallic Ni, associated also with volume shrinkage.

Given the significant impact of porosity on mechanical performance, accurate quantification of porosity is crucial. In each SEM image, the pores on the right half are highlighted in red, illustrating the process by which ImageJ/Fiji identifies the pores based on grayscale contrast. The software then calculates the area fraction occupied by pores, and determines porosity level. Porosity values were statistically evaluated by analyzing 10 randomly selected regions from SEM images of each sample, with the results summarized in Fig. 3.

Fig. 4a shows the average bending strength and elastic modulus values derived from 25 room-temperature bending tests for each BZCY/NiO fuel electrode support subjected to different heat treatment histories. A clear trend emerges from these results, with both average bending strength and elastic modulus showing significant increase as the sintering temperature rises. This enhancement in mechanical properties is attributed primarily to the corresponding reduction in porosity

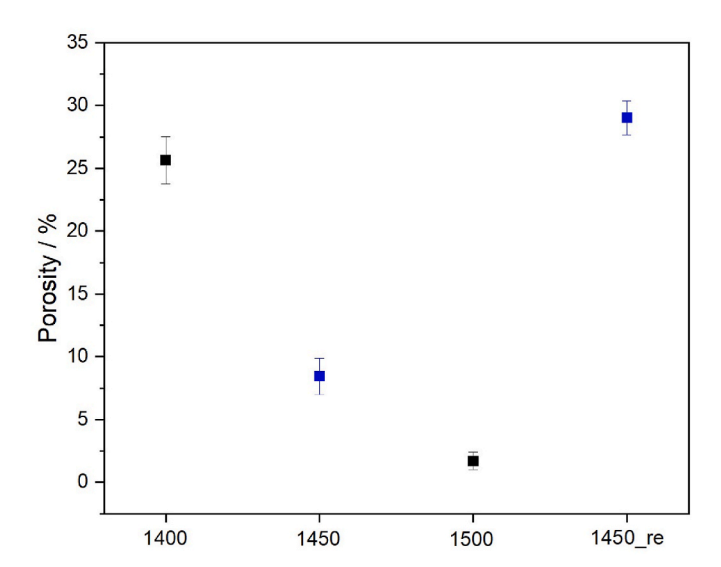


Fig. 3. Porosity variation of BZCY/NiO fuel electrode supports under different thermal treatment histories.

observed at higher sintering temperature, which leads to a denser and structurally more robust material.

Conversely, the sample sintered at 1450 $^{\circ}$ C followed by reduction at 900 $^{\circ}$ C demonstrates a notable decrease in both bending strength and elastic modulus. This decline is attributed to the introduction of porosity due the reduction of NiO to Ni, thereby weakening the overall structure and compromising the mechanical strength of the support. The related mechanical data are listed in Table 1.

Fig. 4b illustrates a strong correlation between the magnitude of bending strength and elastic modulus with the level of porosity. Although various microstructural changes can occur with increasing sintering temperature, porosity appears to be the dominant factor influencing the mechanical performance across the investigated sample

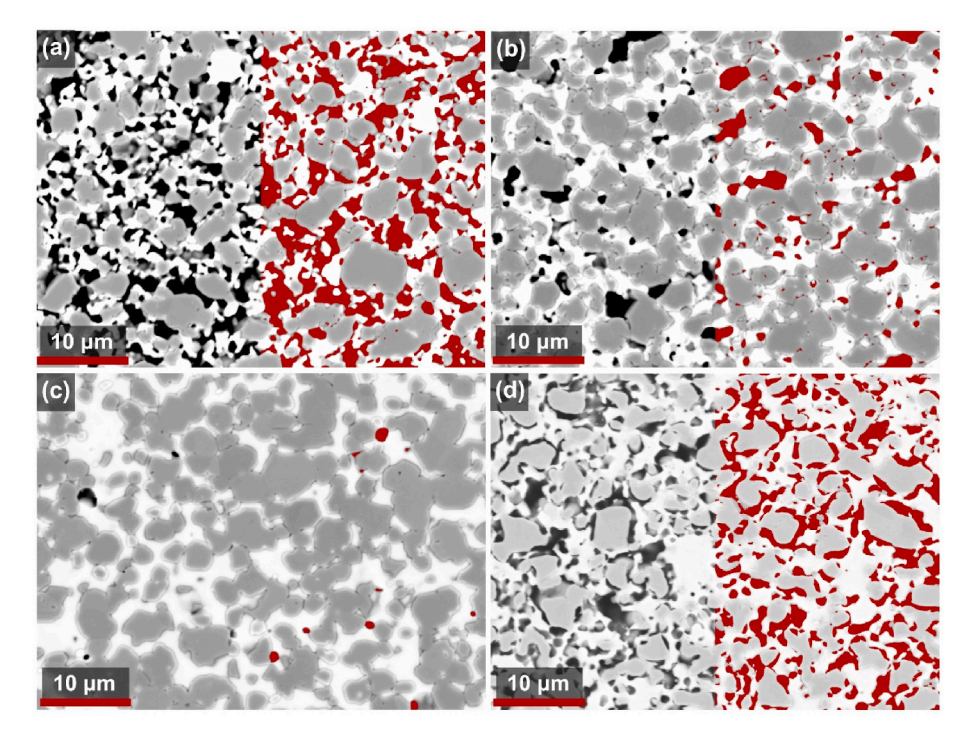


Fig. 2. SEM images of BZCY/NiO fuel electrode supports sintered at 1400 °C, 1450 °C, and 1500 °C (a–c), and after reduction at 900 °C following sintering at 1450 °C (d). In each image, the right half is highlighted in red to indicate the pore regions identified by ImageJ/Fiji software during porosity analysis. (For interpretation of the references to colour in this figure legend, the reader is referred to the Web version of this article.)

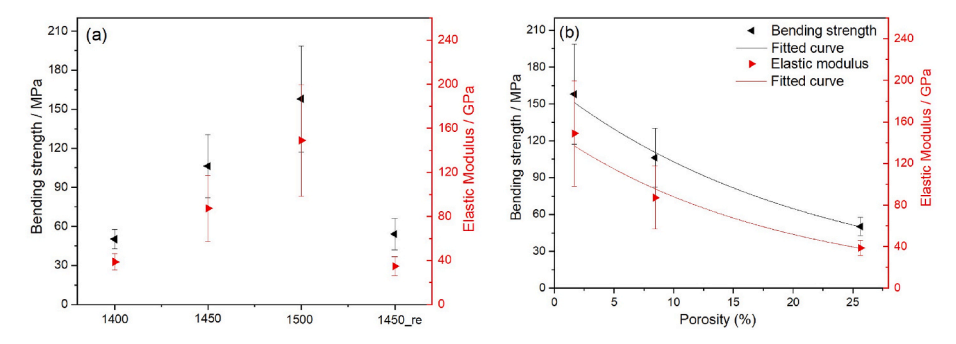


Fig. 4. (a) Bending strength and elastic modulus variation of BZCY/NiO fuel electrode supports under different thermal treatment histories. (b) The dependence of bending strength and elastic modulus on the porosity.

Table 1 Result of the ring-on-ring test at room temperature. E is the elastic modulus. σ_b is the average bending strength. σ_c and m are characteristic strength and Weibull modulus with confidence interval obtained from Weibull analysis.

	Porosity (%)	E (GPa)	σ_b (MPa)	σ_c (MPa)	m	No. Of test
1400	25.6 ± 1.9	39 ± 7	50 ± 7	53 ⁵⁶	$7.6^{9.3}_{5.5}$	25
1450	8.5 ± 1.4	87 ± 30	106 ± 24	116_{108}^{124}	5.3 ^{6.5} _{3.8}	25
1500	1.7 ± 0.7	149 ± 51	158 ± 41	174 ¹⁸⁹ ₁₅₉	$4.3_{3.1}^{5.3}$	25
1450_reduced	29.0 ± 1.4	35 ± 9	54 ± 12	59 ⁶³	5.4 ^{6.7} _{3.9}	25

set. To visualize this macroscopic trend, the porosity dependence of the Young's modulus and bending strength was described by Equations (1) and (2) [29,30]:

$$E = E_0 \cdot \exp(-a \cdot P) \tag{1}$$

$$\sigma_b = \sigma_0 \cdot \exp(-b \cdot P) \tag{2}$$

where E_0 and σ_0 are the elastic modulus and bending strength when the porosity is 0. The experimental data can be fitted with $E_0=149$ GPa, a=

0.05, $\sigma_0 = 163$ MPa and b = 0.05. This empirical fitting is not intended to serve as a detailed physical model but rather to capture a general trend observed in the experimental data. It emphasizes the strong influence of porosity on mechanical strength while acknowledging that other sintering-related factors, e.g., grain connectivity or local composition changes, may also play a secondary role.

Strength is commonly employed as the critical design criterion for the mechanical limits of brittle ceramic materials. However, the measured strength values exhibit significant statistical scatter due to the influence of flaw size distribution. This inherent variability can be

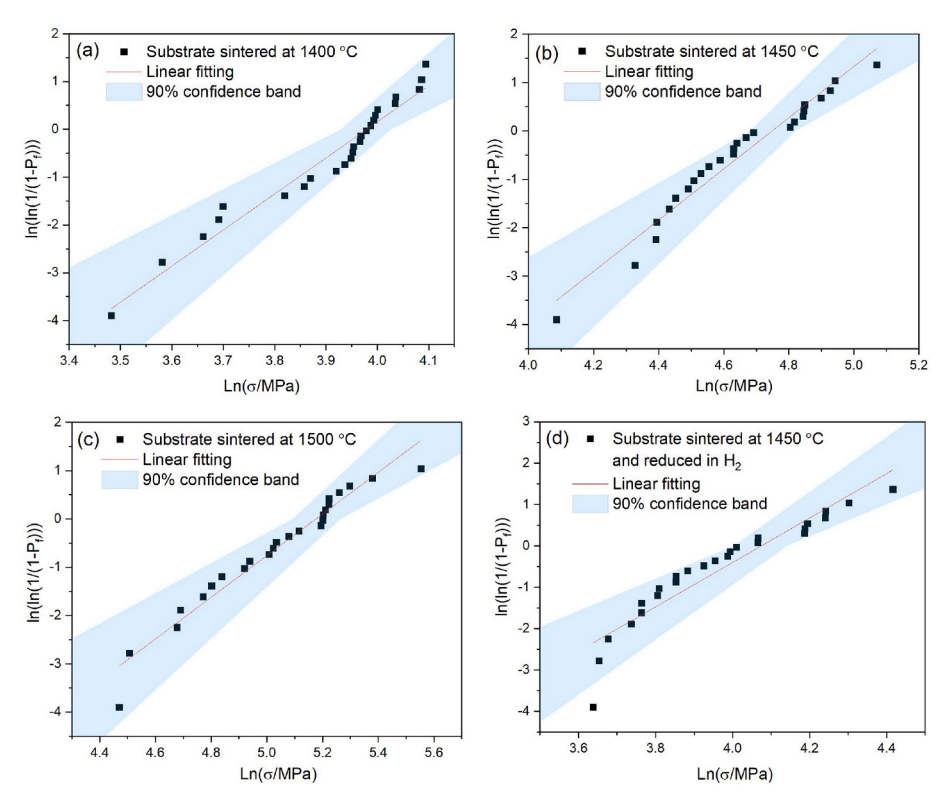


Fig. 5. Weibull plots with confidence intervals. (a)1400, (b) 1450, (c)1500 and (d)1450_re.

effectively characterized by Weibull statistics [31], which has become one of the most prevalent statistical tools for analyzing fracture strength in ceramic materials, particularly for defect-dominated failure mechanisms. The two-parameter Weibull distribution is mathematically expressed as [32]:

$$P_f = 1 - \exp\left[-\left(\frac{\sigma}{\sigma_c}\right)^m\right] \tag{3}$$

where P_f represents the cumulative failure probability at applied stress σ , σ_c denotes the characteristic strength corresponding to 63.2 % failure probability, and m is the Weibull modulus quantifying strength distribution uniformity. A higher m value indicates superior reliability through narrower strength distribution, while lower m values reflect increased strength variability caused by diverse critical flaws.

Fig. 5 presents the Weibull statistical analysis with 90 % confidence intervals for the bending strength of BZCY/NiO(Ni) fuel electrode supports processed under different sintering conditions. The failure probability (P_f) was logarithmically transformed according to classical two-parameter Weibull methodology for linear regression analysis. The derived Weibull parameters in Table 1 reveal an inverse correlation between sintering temperature and Weibull modulus. Specimens sintered at elevated temperatures exhibited decreased Weibull moduli, indicating broader strength distributions.

This trend suggests fundamental microstructural differences that $1400\,^{\circ}\text{C}$ -sintered specimens demonstrated relatively uniform porosity distribution acting as stress-concentrating failure origins, resulting in tighter strength clustering. Conversely, higher temperature processing appears to promote anomalous critical flaws, potentially through exaggerated grain growth or heterogeneous pore coalescence. These irregular defects create weak links in the microstructure, introducing greater strength variability and consequently reducing the Weibull modulus.

To investigate the critical flaws responsible for strength degradation and elucidate the origin of increased strength dispersion in high-temperature sintered specimens, the fracture surface was characterized by SEM, as illustrated in Fig. 6. The fracture surface of specimens sintered at 1400 °C (Fig. 6a) reveals agglomerated BZCY particles without detectable macroscopic pores. When the sintering temperature increased to 1450 °C (Fig. 6b), elongated continuous pores were observed along the periphery of these BZCY agglomerates. This phenomenon became more pronounced with further temperature elevation to 1500 °C (Fig. 6c), where extensive pore networks developed.

The formation mechanism can be attributed to differential sintering rates between the BZCY agglomerates and surrounding matrix particles during thermal processing. This mismatch induces heterogeneous shrinkage, generating localized stress concentrations that evolve into elongated pores. Such pores act as preferential stress concentrators under mechanical loading, serving as critical failure initiation sites. Crucially, the stochastic spatial distribution of these pores introduces

inherent variability in strength-limiting flaw sizes and geometries. This microstructural heterogeneity provides an explanation for both the widened strength distribution and reduced Weibull modulus observed in higher temperature sintered specimens.

To evaluate the operational reliability of BZCY/NiO fuel electrode supports, the high-temperature fracture strength of specimens sintered at 1450 $^{\circ}\text{C}$ was investigated at protonic ceramic fuel cell operating temperatures. Mechanical testing was conducted at 500 $^{\circ}\text{C}$ and 600 $^{\circ}\text{C}$ as well as on reduced-state specimens. Due to the time-intensive nature of high-temperature testing, a limited dataset of three samples per condition was acquired. The measured bending strength and elastic modulus values are summarized in Table 2, with comparative analysis against room-temperature performance.

Notably, both bending strength and elastic modulus exhibited no degradation across the evaluated temperature range compared to ambient conditions. There appears to be even a tendency towards a slight improvement. This anomalous behavior may originate from two potential factors: (1) statistical uncertainty inherent to small sample amount, and (2) thermally induced hydration or dehydration of the BZCY phase that could potentially influence the mechanical performance [33,34]. However, the mechanistic relationship between hydration kinetics and mechanical response remains ambiguous and warrants further investigation. Nevertheless, the results show that the BZCY/NiO substrate is not expected to exhibit special high temperature mechanical failures in the operating condition.

A comparison of the characteristic strengths between 1450 °C-sintered BZCY/NiO and conventional YSZ/NiO oxygen-ion conductor half-cells is summarized in Table 3. Specimens sintered at 1450 °C were selected for this comparative analysis due to their optimal porosity for fuel electrode support applications and compatibility with commonly used co-sintering temperatures for electrolyte integration. Notably, the BZCY/NiO system demonstrates significantly lower bending strength than YSZ/NiO counterparts, particularly in the reduced state. This mechanical deficiency poses twofold challenge: the pre-reduction weakness increases susceptibility to structural failure during manufacturing and stack assembly, while the post-reduction strength degradation raises concerns about long-term operational stability. These observations align with prior reports highlighting low mechanical properties in BZCY/NiO

Table 2 Comparison of the room-temperature and high-temperature mechanical properties of pre-reduction and post-reduction samples sintered at 1450 $^{\circ}$ C.

	Testing temperature (°C)	E (GPa)	σ_b (MPa)	No. Of test
1450	RT	87 ± 30	106 ± 24	25
	500	121 ± 12	137 ± 26	3
	600	87 ± 13	121 ± 6	3
1450_reduced	RT	35 ± 9	54 ± 12	25
	500	33 ± 5	61 ± 13	3
	600	41 ± 12	65 ± 14	3

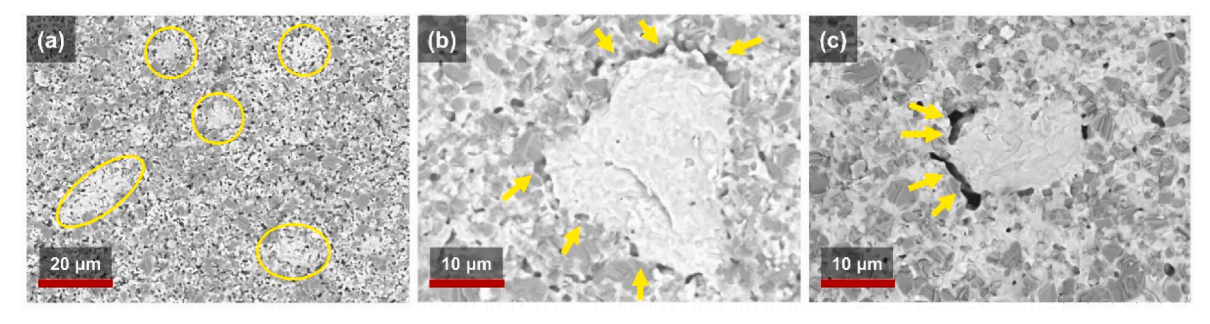


Fig. 6. SEM images of the fracture surface of BZCY/NiO fuel electrode support sintered at (a) 1400 °C, (b) 1450 °C and (c) 1500 °C. The yellow circles in (a) mark the agglomeration of BZCY particles, and the arrows in (b) and (c) mark the elongated continuous pores around the BZCY material phase. (For interpretation of the references to colour in this figure legend, the reader is referred to the Web version of this article.)

Table 3 Comparison of characteristic strengths of BZCY/NiO (1450 $^{\circ}$ C) and conventional YSZ/NiO fuel electrode supports.

Condition	BZCY/NiO	YSZ/NiO [37]	YSZ/NiO [10]
Oxidized	116	175	240
Reduced	59	165	157

substrate [16,17,35]. The bending strength of 50 MPa in our 1400 $^{\circ}$ C sample and 106 MPa in our 1450 $^{\circ}$ C sample is reasonably consistent with the 58.5 MPa reported by Huang et al. [17] and 55.3 MPa reported by Wang et al. [35], given differences in porosity and testing methods. Despite the growing interest in scaling up BZCY-based protonic ceramic electrochemical cells, mechanical reliability remains an under addressed issue that could hinder their technological advancement.

Fractographic analysis in Fig. 6 suggests potential optimization pathways through microstructural engineering. Improved compositional homogeneity achieved via optimized processing parameters may mitigate heterogeneous shrinkage-induced defects. Furthermore, tuning of the Zr/Ce ratio in BZCY could influence sintering behavior [25,36], possibly leading to enhanced mechanical properties, although this remains speculative and requires validation. An alternative approach proposed by Huang et al. [17] involves a bilayer architecture combining YSZ/NiO as the structural support and BZCY/NiO as the functional electrode layer. This hybrid design improves mechanical robustness compared to BZCY/NiO systems while maintaining comparable electrochemical performance.

4. Conclusion

This study presents a comprehensive mechanical evaluation of BZCY/NiO fuel electrode supports for proton-conducting ceramic cells. Both bending strength and elastic modulus increased with higher sintering temperature, primarily due to reduced porosity and improved densification. However, significant mechanical degradation was observed following reduction, attributed to the formation of internal pores resulting from the NiO-to-Ni transformation. Weibull statistical analysis revealed that higher sintering temperatures led to more heterogeneous flaw distributions, reducing mechanical reliability. SEM analysis of fracture surfaces confirmed that abnormal pore networks acted as critical stress concentrators in high-temperature specimens. Despite recent advancements, the mechanical strength of BZCY/NiO remains notably inferior to that of conventional YSZ/NiO systems, particularly in the reduced condition, posing serious challenges for scale-up to stack-relevant sizes and long-term structural stability and reliability. Future efforts should focus on microstructural optimization, compositional tuning (e.g., Zr/Ce ratio), and the development of hybrid support architectures to enhance mechanical robustness in real-world applications.

CRediT authorship contribution statement

Yuan Zeng: Writing – review & editing, Writing – original draft, Validation, Methodology, Investigation, Formal analysis, Data curation, Conceptualization. Jürgen Malzbender: Writing – review & editing, Supervision, Methodology, Data curation, Conceptualization. Olivier Guillon: Writing – review & editing, Supervision, Project administration, Funding acquisition. Mariya E. Ivanova: Writing – review & editing, Supervision, Project administration, Methodology, Investigation, Funding acquisition. Norbert H. Menzler: Writing – review & editing, Supervision, Project administration, Funding acquisition.

Declaration of competing interest

The authors declare that they have no known competing financial interests or personal relationships that could have appeared to influence the work reported in this paper.

Acknowledgement

This study was supported by the Chinese Scholarship Council (CSC) and the Helmholtz Research Program "Materials and Technologies for the Energy Transition" (MTET). Mechanical testing experiments were supported by Ms. Tatjana Osipova (IMD-1).

References

- C. Duan, J. Tong, M. Shang, S. Nikodemski, M. Sanders, S. Ricote, A. Almansoori, R. O'Hayre, Readily processed protonic ceramic fuel cells with high performance at low temperatures, Science 349 (2015) 1321–1326, https://doi.org/10.1126/ science.aab3987.
- [2] W. Bian, W. Wu, B. Wang, W. Tang, M. Zhou, C. Jin, H. Ding, W. Fan, Y. Dong, J. Li, D. Ding, Revitalizing interface in protonic ceramic cells by acid etch, Nature 604 (2022) 479–485, https://doi.org/10.1038/s41586-022-04457-y.
- [3] C. Duan, J. Huang, N. Sullivan, R. O'Hayre, Proton-conducting oxides for energy conversion and storage, Appl. Phys. Rev. 7 (2020) 011314, https://doi.org/ 10.1063/1.5135319.
- [4] H. An, H.-W. Lee, B.-K. Kim, J.-W. Son, K.J. Yoon, H. Kim, D. Shin, H.-I. Ji, J.-H. Lee, A 5 × 5 cm² protonic ceramic fuel cell with a power density of 1.3 W cm⁻² at 600 °C, Nat. Energy 3 (2018) 870–875, https://doi.org/10.1038/s41560-018-0230-0.
- [5] S. Choi, C.J. Kucharczyk, Y. Liang, X. Zhang, I. Takeuchi, H.-I. Ji, S.M. Haile, Exceptional power density and stability at intermediate temperatures in protonic ceramic fuel cells, Nat. Energy 3 (2018) 202–210, https://doi.org/10.1038/ s41560-017-0085-9.
- [6] F. Liu, D. Diercks, P. Kumar, A. Seong, M.H.A. Jabbar, C. Gumeci, Y. Furuya, N. Dale, T. Oku, M. Usuda, P. Kazempoor, I. Ghamarian, L. Liu, L. Fang, D. Chen, Z. Wang, S. Skinner, C. Duan, Redesigning protonic ceramic electrochemical cells to lower the operating temperature, Sci. Adv. 11 (2025) eadq2507, https://doi. org/10.1126/sciadv.adq2507.
- [7] J. Laurencin, G. Delette, F. Lefebvre-Joud, M. Dupeux, A numerical tool to estimate SOFC mechanical degradation: case of the planar cell configuration, J. Eur. Ceram. Soc. 28 (2008) 1857–1869, https://doi.org/10.1016/j.jeurceramsoc.2007.12.025.
- [8] J.H. Yu, G.W. Park, S. Lee, S.K. Woo, Microstructural effects on the electrical and mechanical properties of Ni–YSZ cermet for SOFC anode, J. Power Sources 163 (2007) 926–932, https://doi.org/10.1016/j.jpowsour.2006.10.017.
- [9] S. Biswas, T. Nithyanantham, S. Nambiappan Thangavel, S. Bandopadhyay, High-temperature mechanical properties of reduced NiO–8YSZ anode-supported bi-layer SOFC structures in ambient air and reducing environments, Ceram. Int. 39 (2013) 3103–3111, https://doi.org/10.1016/j.ceramint.2012.09.090.
- [10] J. Wei, T. Osipova, J. Malzbender, M. Krüger, Mechanical characterization of SOFC/SOEC cells, Ceram. Int. 44 (2018) 11094–11100, https://doi.org/10.1016/j. ceramint.2018.03.103.
- [11] L. Blum, L.G.J. de Haart, J. Malzbender, N. Margaritis, N.H. Menzler, Anodesupported solid oxide fuel cell achieves 70 000 hours of continuous operation, Energy Technol. 4 (2016) 939–942, https://doi.org/10.1002/ente.201600114.
- [12] N. Shi, K. Zhu, Y. Xie, D. Huan, J. Hyodo, Y. Yamazaki, Investigation of water impacts on surface properties and performance of air-electrode in reversible protonic ceramic cells, Small 36 (2024) 2400501, https://doi.org/10.1002/ smll.202400501.
- [13] W. Tang, W. Bian, H. Ding, Y. Ding, Z. Zhao, Q. Sun, S. Koomson, Y. Wang, B. Xu, P. Dong, D. Chen, J.Y. Gomez, W. Feng, W. Wu, M. Zhou, Y. Dong, H. Luo, J. Li, D. Ding, Sintering protonic zirconate cells with enhanced electrolysis stability and faradaic efficiency, Nat. Synth (2025), https://doi.org/10.1038/s44160-025-00765-z.
- [14] S. Guo, L. Jiang, Y. Li, P. Zhong, S.A. Ismail, T. Norby, D. Han, From electrolyte and electrode materials to large-area protonic ceramic fuel cells: a review, Adv. Funct. Mater. 32 (2024) 2304729. https://doi.org/10.1002/adfm.202304729.
- [15] H. Yang, Y. Zhang, Z. Liu, C. Hu, J. Li, H. Liao, M. Shao, Hydration-induced stiffness enabling robust thermal cycling of high temperature fuel cells cathode, Nat. Commun. 1 (2025) 3154, https://doi.org/10.1038/s41467-025-57611-1.
- [16] S. Pirou, Q. Wang, P. Khajavi, X. Georgolamprou, S. Ricote, M. Chen, R. Kiebach, Planar proton-conducting ceramic cells for hydrogen extraction: mechanical properties, electrochemical performance and up-scaling, Int. J. Hydrogen Energy 47 (2022) 6745–6754, https://doi.org/10.1016/j.ijhydene.2021.12.041.
- [17] Z. Huang, Y. Yang, H. Lv, C. Shi, Y. Ling, J. Zhou, S. Wang, An interesting application-oriented design of high-strength anode support for protonic ceramic fuel cells by a non-proton-conducting cermet, J. Power Sources 521 (2022) 230989, https://doi.org/10.1016/j.jpowsour.2022.230989.
- [18] H.L. Frandsen, T. Ramos, A. Faes, M. Pihlatie, K. Brodersen, Optimization of the strength of SOFC anode supports, J. Eur. Ceram. Soc. 32 (2012) 1041–1052, https://doi.org/10.1016/j.jeurceramsoc.2011.11.015.
- [19] Y. Xie, Measurement of flexural strengths of SOFC components, SAVE Proc. 2005–07 (2005) 915–922, https://doi.org/10.1149/200507.0915PV.
- [20] D. Miura, Y. Ishida, T. Miyasaka, H. Aoki, A. Shinya, Reliability of different bending test methods for dental press ceramics, Materials 13 (2020) 5162, https:// doi.org/10.3390/ma13225162.

- [21] D.K. Shetty, A.R. Rosenfield, W.H. Duckworth, P.R. Held, A biaxial-flexure test for evaluating ceramic strengths, J. Am. Ceram. Soc. 1 (1983) 36–42, https://doi.org/ 10.1111/j.1151-2916.1983.tb09964.x.
- [22] G. Pećanac, T. Bause, J. Malzbender, Ring-on-ring testing of thin, curved bi-layered materials, J. Eur. Ceram. Soc. 31 (2011) 2037–2042, https://doi.org/10.1016/j. jeurceramsoc.2011.05.021.
- [23] J. Malzbender, R.W. Steinbrech, Fracture test of thin sheet electrolytes for solid oxide fuel cells, J. Eur. Ceram. Soc. 27 (2007) 2597–2603, https://doi.org/ 10.1016/j.jeurceramsoc.2006.11.071.
- [24] Z. Zhong, Stability and conductivity study of the $BaCe_{0.9-x}Zr_xY_{0.1}O_{2.95}$ systems, Solid State Ionics 178 (2007) 213–220, https://doi.org/10.1016/j.ssi.2006.12.007.
- [25] E. Fabbri, A. Depifanio, E. Dibartolomeo, S. Licoccia, E. Traversa, Tailoring the chemical stability of Ba(Ce_{0.8-x}Zr_x)Y_{0.2}O_{3-δ} protonic conductors for intermediate temperature solid oxide fuel cells (IT-SOFCs), Solid State Ionics 179 (2008) 558–564, https://doi.org/10.1016/j.ssi.2008.04.002.
- [26] Y. Zeng, M. Kindelmann, K. Leonard, L.-A. Schäfer, K. Yao, J. Malzbender, M. Müller, O. Guillon, M.E. Ivanova, N.H. Menzler, Characterization of high Zr/Ce ratio Ba(Zr,Ce,Y)O_{3-a} proton conductors: investigating the impact of Y on the properties of materials, Phys. Chem. Chem. Phys. 27 (2025) 885–896, https://doi. org/10.1039/J4CP04384G.
- [27] G. Yan, J.F. Nonemacher, H. Zheng, M. Finsterbusch, J. Malzbender, M. Krüger, An investigation on strength distribution, subcritical crack growth and lifetime of the lithium-ion conductor Li₂La₃Zr₂O₁₂, J. Mater. Sci. 54 (2019) 5671–5681, https://doi.org/10.1007/s10853-018-03251-4.
- [28] J. Malzbender, R.W. Steinbrech, Threshold fracture stress of thin ceramic components, J. Eur. Ceram. Soc. 28 (2008) 247–252, https://doi.org/10.1016/j. jeurceramsoc.2007.05.017.

- [29] E. Ryshkewitch, Compression strength of porous sintered alumina and zirconia: 9Th communication to ceramography, J. Am. Ceram. Soc. 36 (1953) 65–68, https://doi.org/10.1111/j.1151-2916.1953.tb12837.x.
- [30] R.M. Spriggs, Expression for effect of porosity on elastic modulus of polycrystalline refractory materials, particularly aluminum oxide, J. Am. Ceram. Soc. 44 (1961) 628–629, https://doi.org/10.1111/j.1151-2916.1961.tb11671.x.
- [31] J.B. Wachtman, W.R. Cannon, M.J. Matthewson, Mechanical Properties of Ceramics, first ed., Wiley, 2009 https://doi.org/10.1002/9780470451519.
- [32] W. Weibull, A statistical theory of the strength of materials, Proc. Royal 4cademy Engrg Science 1 (1939). https://searchworks.stanford.edu/view/1150953.
- [33] R. Sažinas, M.-A. Einarsrud, T. Grande, Toughening of Y-doped BaZrO₃ proton conducting electrolytes by hydration, J. Mater. Chem. A 5 (2017) 5846–5857, https://doi.org/10.1039/C6TA11022C.
- [34] Z. Wang, Y. Jing, Y. Sun, W. Li, J. Yang, X. Li, Hydration induced mechanical degradation in the Y-doped BaZrO₃ solid oxide, Comput. Mater. Sci. 235 (2024) 112824, https://doi.org/10.1016/j.commatsci.2024.112824.
- [35] Q. Wang, T. Luo, Y. Tong, M. Dai, X.-Y. Miao, S. Ricote, Z. Zhan, M. Chen, Large-area protonic ceramic cells for hydrogen purification, Separ. Purif. Technol. 295 (2022) 121301, https://doi.org/10.1016/j.seppur.2022.121301.
- [36] H.-W. Kim, J. Seo, J.H. Yu, K.S. Yun, J.H. Joo, J. Moon, H.J. Park, Effect of cerium on yttrium-doped barium zirconate with a ZnO sintering aid: grain and grain boundary protonic conduction, Ceram. Int. 47 (2021) 32720–32726, https://doi. org/10.1016/j.ceramint.2021.08.168.
- [37] N.H. Menzler, J. Malzbender, P. Schoderböck, R. Kauert, H.P. Buchkremer, Sequential tape casting of anode-supported solid oxide fuel cells, Fuel Cells 14 (2014) 96–106, https://doi.org/10.1002/fuce.201300153.